Journal of Materials Research and Technology 33 (2024) 9832–9842

Contents lists available at ScienceDirect

Journal of Materials Research and Technology

journal homepage: www.elsevier.com/locate/jmrt

Characterization of the thermal and mechanical properties of additively manufactured carbon fiber reinforced polymer exposed to above-zero and sub-zero temperatures

Isyna Izzal Muna [a], Magdalena Mieloszyk [a,*], Ruta Rimasauskiene [b]

[a] Institute of Fluid-Flow Machinery, Polish Academy of Sciences, Fiszera 14, Gdansk, 80-231, Poland
[b] Department of Production Engineering, Faculty of Mechanical Engineering and Design, Kaunas University of Technology, Studentu 56, Kaunas, 51424, Lithuania

ARTICLE INFO

Handling editor: SN Monteiro

Keywords:
Thermal treatment
Additive manufacturing
Mechanical characterization carbon fiber reinforced polymer structural integrity

ABSTRACT

This experimental work aims to study the thermal degradation of carbon fiber reinforced polymer (CFRP) printed using additive manufacturing. The printed samples were exposed to various thermal modes (prolonged and cyclic) and magnitudes (above- and sub-zero degrees). The influence of temperature on CFRP was investigated using static tensile testing (Young's modulus and tensile strength) supported by scanning electron microscope and differential scanning calorimetry. It is revealed that Young's modulus and tensile strength of samples were all degraded after all thermal treatments. Observing the morphological structure on the surface revealed changes in the degradation processes due to thermal treatments. A list of the dominant degradation types for each analysed thermal treatment is presented in the paper. It was observed that similar mechanical parameters values can be linked with different material degradation processes.

1. Introduction

Additive manufacturing (AM), also known as three-dimensional (3D) printing, has revolutionized the fabrication of complex 3D structures across various industries by enabling the creation of intricate geometries through a layer-by-layer (bottom-up) approach. This contrasts with conventional manufacturing methods that typically employ a subtractive (top-down) technique. Among the numerous applications, carbon fiber reinforced polymer (CFRP) composites have gained significant traction due to their exceptional mechanical properties. These materials are now indispensable in high-performance sectors such as aeronautics [16], automotive [27], civil [26] and marine [19]. Material extrusion, commonly known as Fused Deposition Modeling (FDM), is widely used for creating complex geometries in CFRP composites [2,9]. The benefits of the FDM method are easy-to-use, relatively low budget, and possible parts customization. However, the final elements contain a relatively high amount of voids that negatively influence the mechanical properties of the final product. One of the solutions was designed by Rimašauskas et al. [18]. It is based on the 1 modification of the 3D printer and special preparation of fiber reinforcement before the printing process. The proposed procedure results in enhancing the internal structural integrity due to the better adhesion between fiber bundles inside the laminate.

Continuous carbon fiber (CCF) is increasingly recognized as an optimal reinforcement material for CFRP composites among other carbon fiber types such as short carbon, whiskers, due to its superior strength-to-weight ratio, rigidity, fatigue resistance, and corrosion resistance [3,10]. These properties make CCF an ideal substitute for metals in aerospace structures, enhancing performance while reducing weight. The use of thermoplastics such as polyetheretherketone (PEEK), polylactic acid (PLA), and acrylonitrile butadiene styrene (ABS) as matrix materials further optimizes the manufacturing process by improving melt processability, reducing costs, and eliminating the need for complex curing cycles. This combination has led to the emergence of fiber reinforced thermoplastics as promising materials for various high-performance applications. The advancement of producing CFRP composites as a strong and lightweight structure using AM technology enables printing aerospace parts and implementation in an actual airplane application [14]. The aircraft parts are subjected to prolonged and cyclic mechanical loads and temperature fluctuations ranging from −50 to 150 °C, which can withstand flight at supersonic speeds. In the automotive industry, these settings reflect the thermal loads experienced under prolonged engine heat exposure and varying driving conditions, ensuring the composite can endure stable high temperatures and

* Corresponding author.
E-mail addresses: imuna@imp.gda.pl (I.I. Muna), mmieloszyk@imp.gda.pl (M. Mieloszyk), ruta.rimasauskiene@ktu.lt (R. Rimasauskiene).

https://doi.org/10.1016/j.jmrt.2024.12.028
Received 9 August 2024; Received in revised form 29 November 2024; Accepted 2 December 2024
Available online 4 December 2024

frequent temperature fluctuations without degradation.

Current literature predominantly focuses on the thermal effects on polymeric composites manufactured through conventional methods, leaving a notable gap in the understanding of how 3D-printed CFRP composites respond to similar conditions [1,6,8,12,15,20]. Research has shown varying results, with some studies indicating minor mechanical strength reductions under thermal cycling, while others report significant degradation under prolonged thermal exposure. Lafarie-Frenot and Ho [8] carried out an experimental work on a carbon/epoxy laminated plate $[0_3/90_3]_s$ subjected to 1000 thermal cycles (−50 to 150 °C) under nitrogen or oxygen. It was found that the specimens were gradually damaged by transverse matrix cracks which accumulated and propagated during the test. The results showed that the orientation of the edges referred to as fibers and the layer locations within the lay-up have a significant impact on the transverse matrix cracking of composite laminates subjected to heat cycles. Handwerker et al. [6] found that applying heat to fiber reinforced polymer (FRP) composites improved their mechanical properties such as stiffness and interlaminar strength in the build-up orientation even though the microscopical analysis showed that the test samples still contained a big ratio of air and void. Annealing the parts for 6 h at 200 °C, which is the melting point of Polyamide 6 (PA6) as the used matrix material, produced the best results.

Pascual-González et al. [15] attempted to decrease the porosity content in the CFRP composites with the same thermoplastic material PA6, using post-processing temperature. It was revealed that without changing dimensional sizes, the treated parts subjected to 150 °C improved interlaminar strength by 145% and reduced porosity by approximately 87%. Abdullah et al. [1] revealed that after thermal cyclic exposures, the material possesses a small decrease in mechanical strength. The tensile strength of the tested samples decreased as the number of thermal cycles increased. Tensile properties decreased after 5600 thermal cycles by up to 8.5% when compared to the untreated sample group.

In this experimental research, those research gaps are being studied by examining the mechanical and thermal properties of CFRP composites fabricated with a modified FDM printer. By subjecting the 3D-printed samples to prolonged and cyclic thermal treatments, both above and below 0 °C, this research will employ techniques such as tensile testing, differential scanning calorimetry (DSC), scanning electron microscopy (SEM), and optical imaging to evaluate the mechanical behavior of the composites and their structural integrity. The findings will enhance the understanding of degradation processes and provide insights into optimizing the manufacturing and treatment of 3D-printed CFRP parts for high-performance applications in aerospace, automotive, and other industries.

2. Materials and 3D-printing method

2.1. Materials

In this experimental work, unidirectional (UD) CFRP composites were manufactured with the modified FDM printer MeCreator2 at Kaunas University of Technology, Lithuania according to the procedure designed by Rimašauskas et al. [18]. The matrix agent was thermoplastic PLA (Polymaker), and the CCF reinforcement was T300D-3000 (Toray, France) with 3000 carbon fiber tow. Table 1 displays the matrix and fiber mechanical properties based on information from material suppliers. A total of 45 3D-printed CFRP samples were produced, with the 3D-printed specimens illustrated in Fig. 1. Each specimen was designed with dimensions of 150 × 13 × 2 mm, and the carbon fiber content in the composite was approximately 18.2%. This estimated fiber content was determined based on the tool-path length used during printing and can be measured as the weight ratio of carbon fiber to the overall composite specimen [23]. This method provides a precise estimation of the carbon fiber distribution within the matrix.

Table 1
Mechanical properties of composite components.

	Elastic modulus (GPa)	Elastic strength (MPa)	Strain at failure (%)	Density (g/cm^3)
Matrix	2.636	46.6	1.9	1.17
Fiber	230	3530	1.5	1.76

2.2. Printing process and parameters

Pre-impregnation procedure was used for the reinforcement using CCF to improve the printing performance and filament bonding. PLA pellets were dissolved in a 90 g/10 g dichloromethane solution from Euro-chemicals using a magnetically charged LBX H01 mini-stirrer at 600 rpm. The virgin CCF tow (non-impregnated) was run through this polymer and concurrently dried using an air gun at 220 °C.

The extrusion printing head has been modified with two inputs (one for the fiber component and one for the matrix material) and one output, enabling the material made from polymers to be fused with the fiber throughout the printing process. The impregnated CCF was fed directly to the printing nozzle through the printing head. Liquid PLA is joined with impregnated CF and pumped continuously through the printing nozzle while the polymer melts inside the mixing chamber of the heating control unit. The modified FDM printer device and configuration of the 3D-printed specimen are presented in Fig. 2.

The optimal temperature at the printing head for melting PLA and creating a bond with CCF was 220 °C. The PLA material reinforced with carbon fiber is extruded through the printing nozzle on the borosilicate glass printing bed that is mounted on the Al plate. The rectilinear pattern of the printing process was selected, and the extrusion width was set to be 1.4 mm forming nine continuous parallel lines in each deposited layer. The layer height was set to have four layers for each 3D-printed specimen. After printing the composite sample, the cutter will separate the filament spool and the 3D-printed part. The borosilicate glass should be removed from the Al plate bed to cool before extracting the 3D-printed sample with blades. The printing process parameters are shown in Table 2.

3. Experimental methods and equipment

3.1. Thermal treatment

After manufacturing, nine groups of 3D-printed CFRP specimens were thermally exposed at different magnitudes (above and subzero degrees Celsius) and exposition times (cyclic and stable). Table 3 presents the sample groups under various thermal conditions. Within each thermal group, there are five individual specimens, providing a sufficient sample size to ensure accurate and reliable testing results. This approach is crucial for understanding how varying thermal exposures influence the mechanical behavior of CFRP materials. It is important to note that thermal treatments at temperatures above zero degrees Celsius are referred to as hot thermal treatments, while those below zero degrees Celsius are referred to as cold thermal treatments.

For hot thermal group, the experimental work was conducted at Kaunas University of Technology, Lithuania, with a universal environmental oven, “Memmert” Model UFB-400. This oven provided a constant renewal of oxygen from ambient air. The temperatures in the hot thermal loading were selected to ensure they remain above the glass transition temperature (Tg) yet below the melting temperature (Tm) of PLA polymer as matrix material used in the specimens which are about 60 °C and 160 °C, respectively. For the hot stable group, the specimens were placed in a preheated oven at a desired temperature and duration (e.g., 65 °C 6 h) and allowed to cool naturally to room temperature afterwards.

For the hot cyclic group, the temperature cycles were manually

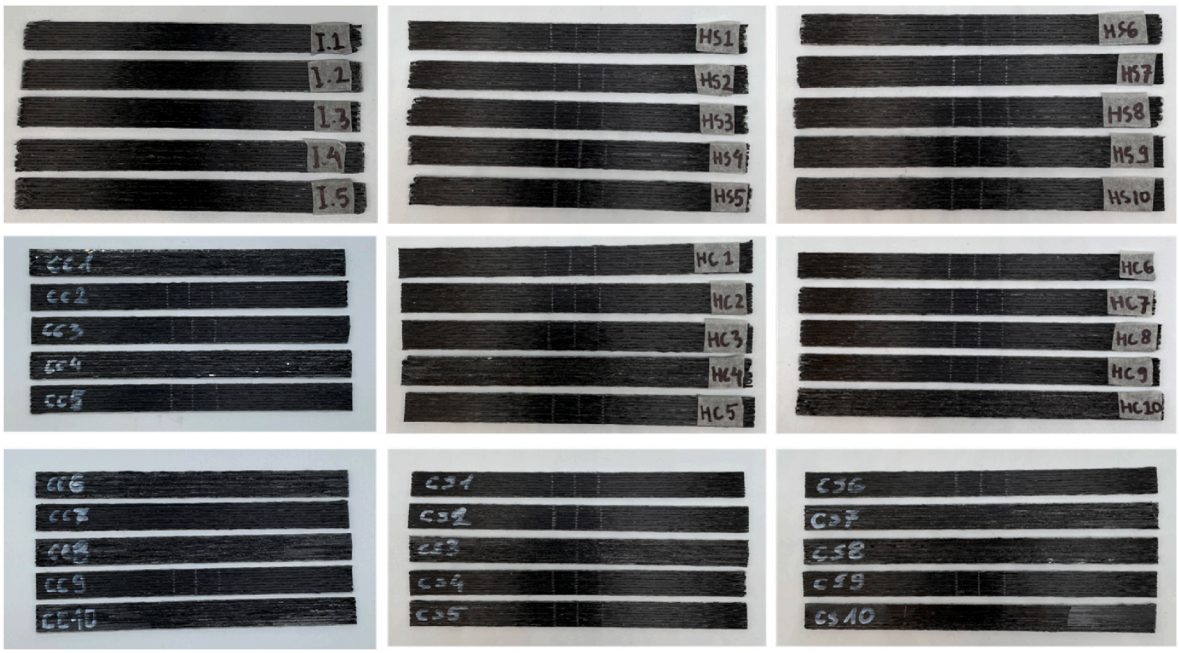

Fig. 1. AM CFRP specimens printed with a modified FDM printer prior to thermal and mechanical testing.

regulated using the controller settings of the oven, based on real-time thermocouple readings. The specimens were subjected to multiple thermal cycles within a specific temperature range (e.g., between 50 and 70 °C for six cycles) according to a thermal cyclic plan. Each cycle included two sets of temperatures, with a 10-min dwell time, a cooling rate of 2.5 °C per minute, and a heating rate of 1 °C per minute. The heating rate was manually controlled and monitored through thermocouple feedback to maintain accuracy. The cooling process occurred naturally, with the heat source turned off and the cooling rate carefully observed. For the cold thermal group, the experimental condition was performed at the Institute of Fluid-Flow Machinery, Polish Academy of Sciences, Poland with an automated environmental chamber "MyDiscovery" model DM600C (Angelantoni Test Technologies Srl, Italy).

For the cold stable group, the specimens were placed in a chamber at programmed temperatures and duration before being naturally cooled to room temperature. For the cold cyclic group, the environmental chamber was automatically regulated for a specific temperature range and several thermal cycles following the thermal cyclic plan. Each cycle had two desired temperatures with 10 min of dwelling time, a cooling rate of 5 °C per minute, and a heating rate of 2 °C per minute. The environmental chamber and oven are presented in Fig. 3. The environmental chamber parameters are shown in Table 4.

The temperatures for the cold thermal loading in this experiment were selected to mimic the thermal conditions experienced by aerospace components during high-altitude flights and space missions. At such altitudes, aerospace structures, including satellite bodies and other high-performance materials, can be exposed to temperatures that dip significantly below freezing, especially when transitioning from direct sunlight to the shadow of Earth or other celestial bodies. The testing protocol for cold thermal loading followed the MIL-STD-883 standard, specifically Method 1010. The −20 °C threshold is commonly chosen as a balance between reflecting the extreme cold conditions experienced and considering the potential impact on mechanical integrity, without exceeding the operational temperature limits of the material [22].

Several studies have explored the impact of temperature gradients, such as 5 °C or 10 °C, in evaluating the effects of temperature cycling on the properties of CFRP material [4,21,24]. A temperature gradient of this scale, often used in experimental setups, crucial for understanding how materials respond to thermal stress over repeated cycles. For example, gradients of 10 °C allow researchers to assess the expansion and contraction behavior of materials, simulating conditions like thermal fatigue and the thermal expansion mismatches that occur in real-world applications [4,24].

It is important to note that the time experienced by samples treated at prolonged above and sub-zero degrees is consistent, but for cyclic temperatures, it varies due to the differences in temperature range. It is worth mentioning that the CFRP sample maintained its shape during the 6-h treatment at 145 °C, despite this temperature being close to the melting point of PLA, primarily due to the reinforcing role of carbon fibers. These fibers provide significant structural integrity and mechanical strength, preventing the PLA matrix from deforming significantly. Carbon fibers also aid in evenly distributing heat throughout the composite, reducing the risk of localized overheating and deformation.

3.2. Surface analysis

SEM and optical microscopy analysis were carried out to evaluate the microstructure and macrostructure of specimens due to thermal treatment. The optical microscope, Nikon Eclipse LV100ND, was used to examine the micro-morphological structures outfitted with a high-definition color camera (Nikon DS-Ri2). The data was prepared and processed using imaging software (NIS Elements 4.5.1.00, Nikon Europe B.V., Amstelveen, The Netherlands). The largest sample size seen under the optical microscope was 150 mm square. A scanning electron microscope (FE-SEM SU5000, Hitachi Co., Tokyo, Japan) was utilized to observe the micro-damage that resulted from tensile testing on various specimen groups. The largest specimen that the SEM could measure had dimensions of 80 mm × 200 mm. The study used a digital microscope with 500× magnification (Levenhuk, DTX 500 LCD, Warsaw, Poland).

3.3. Thermal analysis

DSC measures the energy absorbed (endotherm) or released (exotherm) as a function of time or temperature and it is suitable for detecting the effects of thermal degradation by observing the melting and crystallization process. The important thermal phases are studied to determine the polymer crystallinity: glass transition temperature (Tg) following ASTM standard E1356, cold crystallization (Tcc), and melting

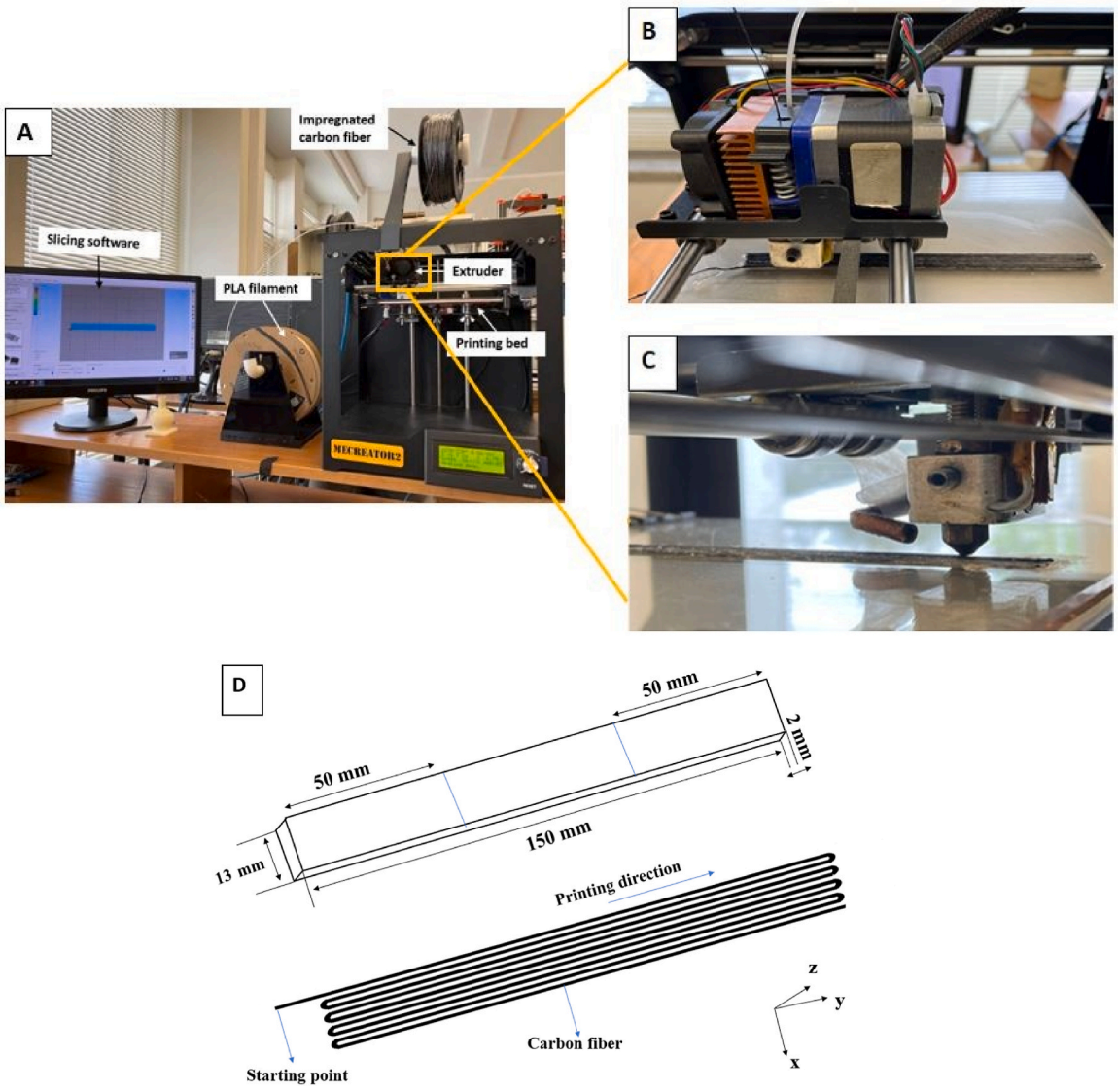

Fig. 2. 3D-printing setup of the modified FDM printer and filament spools (A); extruder (B); printing nozzle (C); 3D-printed specimen configuration (D).

Table 2
Printing parameters.

Parameter	Value
Nozzle temperature	220 °C
Bed temperature	90 °C
Interior infill	100%
Infill pattern	Rectilinear
Printing speed	3 mm/s
Nozzle diameter	1.5 mm
Extrusion multiplier	0.7
Primary layer height	0.5 mm

Table 3
Sample groups.

Group name	Description
Intact	Untreated samples
HS-A	Hot stable at 65 °C for 6 h
HS-B	Hot stable at 145 °C for 6 h
HC-A	Hot cyclic between 50 and 70 °C with 6 cycles
HC-B	Hot cyclic between 140 and 150 °C with 6 cycles
CS-A	Cold stable at 0 °C, for 6 h
CS-B	Cold stable at −20 °C, for 6 h
CC-A	Cold cyclic between −5 and 0 °C for with 12 cycles
CC-B	Cold cyclic between −20 and −15 °C with 12 cycles

point (Tm) temperatures following ASTM standard E794. Tg is indicated by a shift of the baseline from the initial DSC curves and reported Tg was based on the observed midpoint temperature. An exothermic peak indicates a cold crystallization where an exothermic reaction (heat release) occurs, while an endothermic peak (heat adsorption) refers to the melting temperature in which an endothermic reaction takes place.

A DSC equipment, TA Instruments Q2000, was utilized to analyze the thermal properties of CFRP specimens under controlled and isothermal conditions. The sample for each thermally treated group was chopped into small pieces and measured with a precision scale. About 10 mg of sample from each treatment group was placed in an Al hermetic pan and inserted into the DSC cell. A nitrogen atmosphere was supplied to the test chamber at a flow speed of 50 mL/min for the cooling process, while an electrically heated furnace was used for heating. The DSC measurement for each sample consisted of two times of the heating process and one time of the cooling process. The first heating scan in DSC is used for removing the thermal history of the polymer which might have gone through during its synthesis and post-processing steps. Tg value difference after the second heating run could be insignificant whereas Tm and

Fig. 3. An automated environmental chamber for cold thermal treatment (left) and an air-circulated oven for hot thermal treatment (right).

Table 4
Environmental chamber parameters.

Parameter	Value
Temperature [°C]	−75 ÷ 180
Temperature fluctuations [°C]	±0.1 °C ÷ ± 0.3 °C
Temperature change rate [°C/min]	
Heating	4.5
Cooling	4
Relative humidity [%]	10 ÷ 98
Relative humidity fluctuations [%]	1 ÷ 3

Tc value difference could be very distinct difference in their respective values between the two runs. The DSC program is shown in Table 5.

A DSC measuring cell consists of a furnace and an integrated sensor with designated positions for the sample and reference pans. The sample is placed in an Al pan, and the sample pan and an empty reference pan are placed on small platforms within the DSC chamber. Thermocouple sensors lie below the pans and they are connected to thermocouples. This allows for recording both the temperature difference between the sample and reference side (DSC signal) and the absolute temperature of the sample or reference side. The functional principle of an interior chamber of DSC is shown in Fig. 4.

DSC was used to determine the glass transition temperature (Tg) of the polymeric composite samples in accordance with ASTM E1356. The melting temperature and crystallization temperature will also be analysed according to ASTM E794. The purpose of the test was to determine whether there was any change in the crosslinking of the PLA polymer, which could signify degradation as a result of the conditioning process. A DSC equipment (TA Instruments Q2000) was used to perform thermal analysis of the composite samples under controlled and isothermal conditions. The sample for each thermally treated group was chopped into small pieces to fit inside the pan due to the stiffness of the fiber-reinforced raw filament.

Table 5
DSC program steps.

Step	Temperature [°C]	Heating rate [°C/min]
Hold equilibrium	24	
Ramp-up	200	10
Hold isotherm for 2 min		
Ramp-down	40	10
Hold isotherm for 2 min		
Ramp-up	200	10

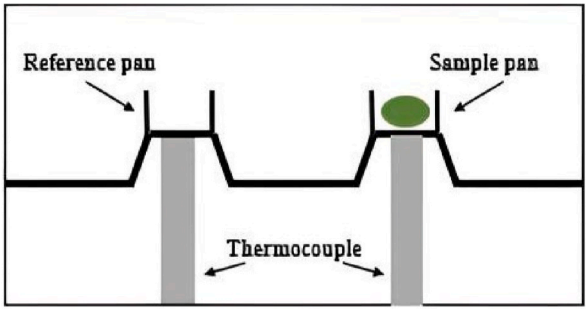

Fig. 4. Schematic diagram of DSC interior chamber.

One representative sample was prepared for each treatment group in the DSC analysis. The prepared samples were cut into small workpieces with a weight of about 10 mg for each sample. Each cut sample then was placed in an Al hermetic pan and inserted into a DSC cell. A nitrogen atmosphere was supplied to the test chamber at a flow rate of 50 mL/min for the cooling process while an electrically heated furnace is used for heating. The temperature was ramped from 20 to 200 °C and then cooled back to 20 °C at a heating and cooling rate of 10 °C/min. The measurement for each sample consisted of two times of the heating process and one time of the cooling process. The following program was used: hold equilibrium at 24 °C, ramp at 10 °C/min to 200 °C, hold isotherm for 2 min, ramp at 10 °C/min to 40 °C, hold isotherm for 2 min, and ramp back at 10 °C/min to 200 °C. The DSC equipment and DSC cell can be seen in Fig. 5.

3.4. Mechanical testing

After thermal treatment, tensile testing was carried out on a Tilnius Olsen H25KT universal testing machine with hydraulic grips of 25 kN. An extensometer was calibrated with a displacement rate of 2 mm/min against strain gauges to determine tensile strength and strain for all group samples. Four locations on the samples were labelled with a marker 15 mm from the center to measure the elastic strain. Gripping tabs made of PLA were printed separately, having dimensions 50 mm in length, 12.5 mm in width, and 2 mm in thickness, and each specimen was then glued with two tabs at the front side and two at the backside. Five samples for each group of thermal treatment were required to determine the mean value for the mechanical properties of the specimens according to the ASTM D3039 standard. The specimen prepared

Fig. 5. DSC equipment and DSC cell.

for tensile testing and tensile test setup are shown in Fig. 6.

The ASTM D3039 standard was used for calculating the modulus of elasticity (Young's modulus) in materials testing. The tensile modulus and strength values of the CFRP specimens were calculated by Equation (1) and Equation (2), respectively.

$$\sigma = \frac{F_{max}}{A} \tag{1}$$

$$E = \frac{\Delta F\, L_0}{A_f\, \Delta L} \tag{2}$$

where F_{max} denotes the maximum tensile force given during the test (N), A_f is the cross-sectional area of the composite specimen (mm^2), ΔF and ΔL are the differences in the force and extension between two strain points, respectively, and L_0 is the gauge length of the specimen.

4. Results and discussion

The DSC results, tensile testing, and SEM analysis will be presented in this section.

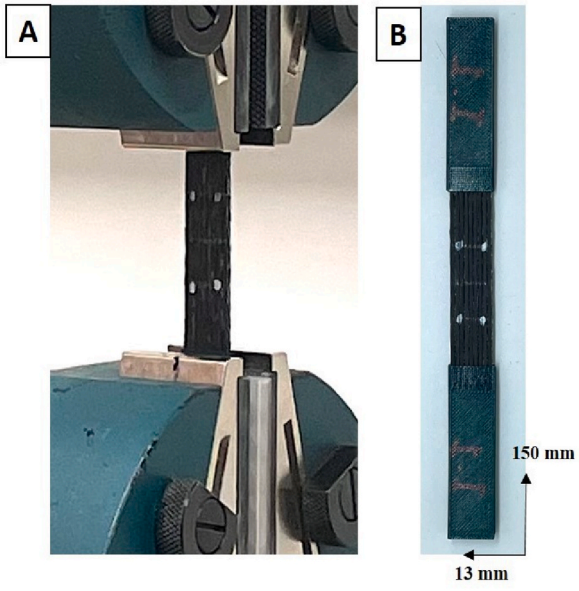

Fig. 6. Tensile testing setup (A); and CFRP specimen with tabs (B).

4.1. Thermal analysis

The mechanism of the heating process between the reference pan and the sample pan is presented in Fig. 4. When the DSC measuring cell is being heated, the reference side—typically an empty pan—heats up more quickly than the sample side because of the sample's heat capacity (C_p); for example, the reference temperature (Tr, green) rises slightly more quickly than the sample temperature (Ts, green). The two curves behave similarly while heating at a steady rate until a sample reaction occurs. In this example, the sample melts at t_1. The temperature of the sample does not vary during melting; nevertheless, the temperature of the reference side remains constant and continues to rise linearly. When melting is complete, the sample temperature begins to rise again, with a linear increase commencing at time t_2.

The DSC curves for the initial heating, cooling, and second heating cycles of intact (untreated) and thermally treated CFRP specimens at prolonged and cyclic temperatures are shown in Figs. 7 and 8, and the values obtained from the tests are shown in Table 6.

In the first heating process, the Tg of the untreated (intact) CFRP group is very close to composites treated in a stable temperature at 0 °C (CS-A) and −20 °C (CS–B), as well as cyclic temperatures between 0 and 5 °C (CC-A). Similar values of Tg were also observed for specimens subjected to cyclic heating (HC-A and HC-B). This means that these groups will take a longer time to change their material state from solid to a soft-rubbery material after the thermal treatment which makes them more brittle.

However, with thermal cycling at extremely low temperatures between −20 and −15 °C (CC–B) and stable high temperatures (HS-A and HS-B) the Tg value noticeably dropped.

The Tcc point of the intact group and CS-A are significantly higher than for the other treated groups. Cold crystallization is the process of rapidly cooling a crystalline plastic from its liquid state, resulting in the freezing of polymer chains in their amorphous state. Crystallization is characterized by crystal nucleation and nucleus growth [25]. However, cold crystallization did not occur for the higher magnitude of hot thermal treatment where the specimens were exposed to cyclic temperature (HC–B) and stable temperature (HS–B). This happens because the crystals do not have enough time to form. The formation of crystals creates an endothermic peak between the Tg and the melting point when reheating a material in this state. The cold crystallization process is distinguished by two characteristics the promotion of nucleation as the supercooled glassy state gradually gains mobility with increasing temperature and the presence of a maximum temperature for nucleation above which the cold crystallization process is diffusion limited [13].

It was observed that all sample groups had a double melting temperature peak during the first heating run. This is owing to the superpositioning of melting and recrystallization processes, which causes this phenomenon. When most crystallization occurs during the cool-down process, the remaining amorphous regions lack place and chain mobility, resulting in defective crystals. These defective crystals begin to melt, but almost simultaneously, recrystallization occurs, generating a new crystal structure that melts almost quickly, creating the second peak [6].

During phase transitions, CFRP samples exhibited two distinct peaks (and onset points), which may indicate more than one form or crystal structure. PLA has slow crystallization kinetics. In the case of PLA, three different crystallization processes can be identified with adequate experimental conditions: the classical cold crystallization and two processes associated with the non-reversing exotherms [5]. The DSC graphs obtained in this experiment exhibit unexpected and extraneous results, such as non-reversing heat-flow curves with two exothermic processes and a larger endotherm in the middle. The multi-exothermic processes result from several crystalline states of PLA (α and β).

The DSC curve produced lower values in the second heating process than in the first run. This phenomenon is because the relaxation or molecular rearrangement already occurred in the first heating run. The

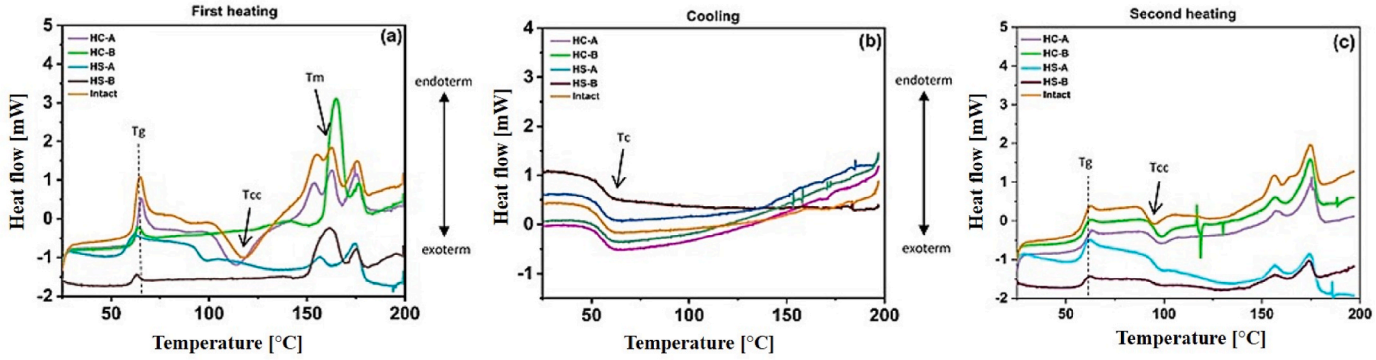

Fig. 7. DSC graphs of thermally treated and non-treated 3D-printed specimens for above-zero degrees treatment groups: (a) First heating; (b) Cooling; (c) Second heating.

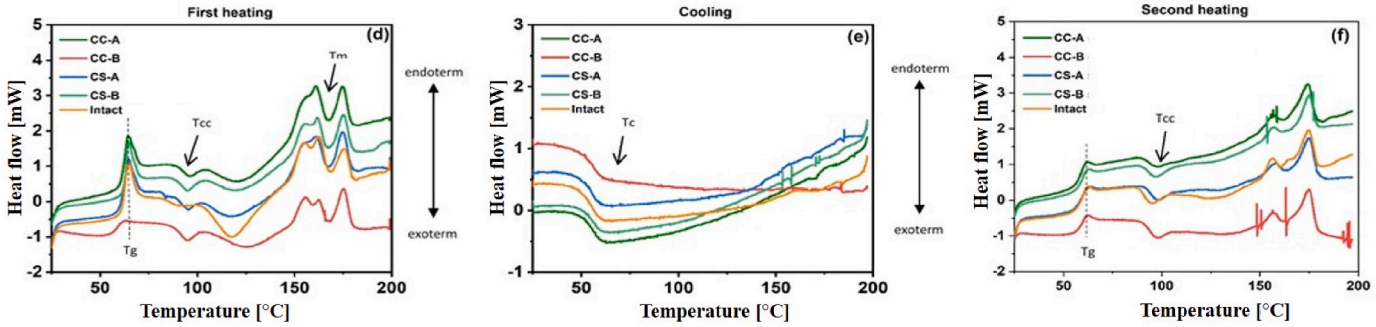

Fig. 8. DSC graphs of thermally treated and non-treated 3D-printed specimens for sub-zero degrees treatment groups: (d) First heating; (e) Cooling; (f) Second heating.

Table 6
DSC results of CFRP composite samples.

Group name	Glass transition temperature Tg [°C]	Cold crystallization temperature Tcc [°C]	Melting temperature Tm [°C]	Crystallization temperature Tc [°C]
Intact	64.88	118.67	158.09	60.80
HS-A	61.58	98.29	162.91	60.07
HS-B	63.23	–	161.39	59.8
HC-A	65.43	114.38	157.82	58.97
HC-B	64.19	–	164.83	59.66
CS-A	64.73	118.07	157.89	59.02
CS-B	64.61	94.88	158.92	59.93
CC-A	64.33	95.68	159.06	58.42
CC-B	62.55	94.72	158.64	60.76

cooling process imparts/equilibrates the previously known history at a known rate from the first heating before heating again. As a result, any changes detected in the reheating curve between identical materials are not due to previous thermal history effects but rather the differences in the actual internal materials (e.g., molecular weight).

In the cooling cycle, the melt crystallization peak for each sample group can be observed and determined by the peak, which denotes the crystalline nature of the polymer. However, there are some cases when the reinforcement materials constrain the PLA chains so much that the heat capacity jump becomes undetectable in DSC. Nucleation on the sample borders, regional confinement, temperature gradient, and melt flow are all important aspects of polymer crystallization. Similarly, foreign chemicals in the pure PLA matrix affect PLA crystallization by facilitating or impeding chain movement. Furthermore, due to the presence of ordered crystallites and thicker lamellae, higher crystallinity generates higher stiffness in both materials, preventing the material from slipping into the crystal blocks [7]. In contrast, reduced crystallinity produces a higher ductility with reduced strength and stiffness [17,29].

4.2. Mechanical characterization analysis

Fig. 9 depict the typical stress-strain curves obtained from the tensile tests of CFRP composites of the above-zero and sub-zero degrees group, respectively. While some graphs depict a trend of linear elasticity, others began to break at elongation. This type of behavior is common in semi-crystalline polymers. When the yield strength is exceeded, the chains in the amorphous sections straighten out and stop interconnecting with one another [6].

The tensile stress-strain graphs show that the untreated composite specimen reached the highest stress level, followed by the prolonged temperature group exposed to 65 °C. The lowest stress level was attained from a specimen group subjected to a cyclic temperature between 50 and 70 °C with a considerable strain level indicating more elasticity. The premature failure of 3D-printed samples at a strain of 0.75%, despite the higher elongation at break for each constituent of fiber and PLA (>1%), is likely due to a combination of processing defects like voids and porosity, stress concentrations from geometric irregularities, residual stresses from the thermal history of printing, and the inherent anisotropy of the 3D-printed composite structure. These factors collectively contribute to a lower effective strain capacity of the 3D-printed samples compared to the individual materials.

The corresponding mechanical parameters (Young's modulus and tensile strength) are shown in Fig. 10. The untreated samples showed the highest tensile strength mean and Young's modulus. The tensile properties of specimens then decreased after various modes of thermal treatment at different temperature ranges. For the stable thermal treatment, the sample group treated to the above-zero temperature

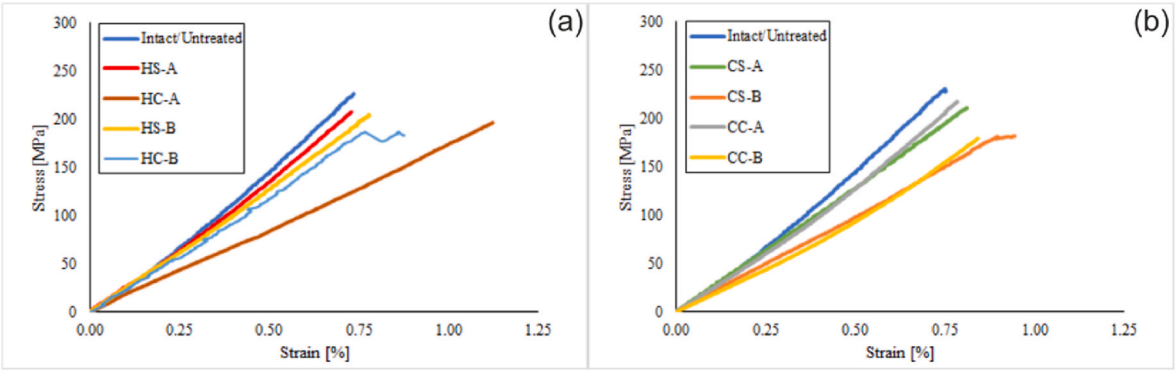

Fig. 9. Average stress-strain curves for thermal treatment group: (a) above-zero, (b) sub-zero.

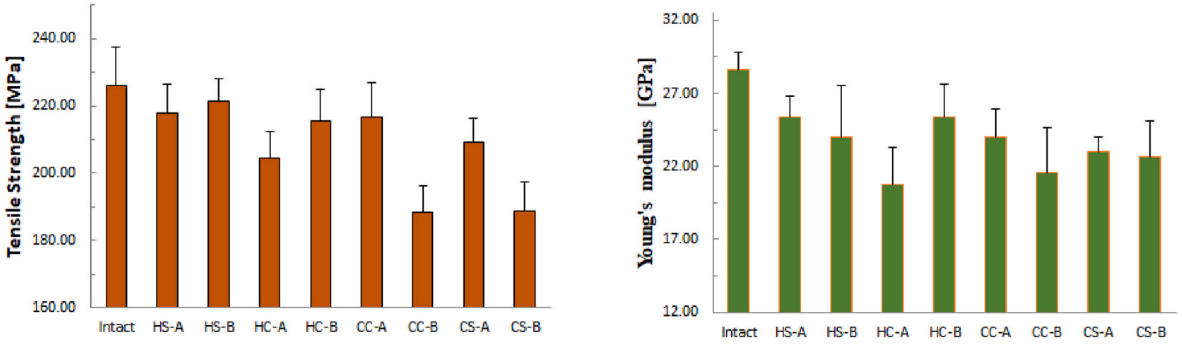

Fig. 10. Experimental results of the tensile strength and Young's modulus of 3D-printed samples for all thermal treatment groups.

achieved higher ultimate tensile strength than the sub-zero temperature. The lowest Young's modulus and ultimate tensile strength were obtained from the sample group treated at −20 °C. Treatment at 65 °C significantly reduced the ultimate tensile strength and Young's modulus. However, at 145 °C Young's modulus was reduced but the ultimate tensile strength appeared to be slightly higher than the treated sample at 65 °C.

The mean values in the bar plots represented the patterns of each printed group specimen and the range of their effects on tensile qualities. It is assumed that the decrease in mechanical strength and elastic modulus under thermally stable and cyclic loading was caused by the difference in coefficients of thermal expansion (CTE) between the matrix and fiber [11]. The material degraded due to the thermal stress caused by the CTE disparity, which might lead to fibers pulling out due to fiber-matrix debonding. The deviation in the mechanical properties observed in the results can be attributed to the inherent variability in the 3D-printing process, particularly when using a modified 3D printer for CFRP samples. This type of 3D printer, while capable of 3D-printing CFRP composites, often faces challenges related to repeatability in terms of both the quality and dimensions of the printed samples.

The tensile tests results (reduction of Young's modulus and tensile strength) are consistent with the DSC findings, where reduced thermal stability (lower Tg) and altered crystallinity were observed. The different levels of crystallinity between sample groups can help explain the observed mechanical differences. Furthermore, in the research study of thermosetting systems [28], crystallization behavior can be analysed similarly in thermoplastic-based composite systems. In these systems, the post-manufacturing crystallization is crucial, where residual thermal conditions continue to affect the crystalline content and, in turn, the material's final mechanical performance. The degree of crystallization post-processing can influence the toughness and load-distribution capabilities of the composite, just as in thermosetting polymers where cross-linking determines the final properties.

4.3. Morphological analysis

Before and after the thermal loading exposures, morphological studies were carried out using an optical microscope device, and the microstructure of the various specimen groups after tensile testing was investigated using a scanning electron microscope.

4.3.1. Optical microscopy

Fig. 11 presents the surface structure at the microscopic scale from each heating group before and after thermal loading. This optical analysis was solely conducted at elevated temperatures due to its direct correlation with the thermal treatment procedure proposed post-manufacture. The PLA matrix material looked slightly finer and smoother on the prolonged and cyclic treatment samples at lower temperatures (HS-A and HS-B). However, these specimens showed no distorted shapes (some crease structure along specimen length) because of insufficient high-temperature exposure. The thermal treatment at higher temperatures showed a more obvious difference on the surface after the treatment [12].

The CFRP sample subjected to continuous heating at 145 °C reveals significant drying out of the polymer matrix. This thermal exposure causes a reduction in the moisture content of the matrix, leading to changes in its physical properties. This change is evident in the DSC results, where the melting peak area is notably reduced. The smaller area under the melting peak indicates a decrease in the thermal energy required for phase transitions, which is consistent with the loss of volatiles and moisture from the polymer matrix during prolonged heating.

4.3.2. Scanning electron microscopy

The samples after tensile testing were examined using SEM. Micrographs are presented in Fig. 12. The polymer structure of the he untreated sample shows no signs of breakage or deterioration. Upon close examination, it exhibits a pristine surface with no observable defects or flaws. PLA subjected to cyclic heating between 50 and 70 °C (HC-A)

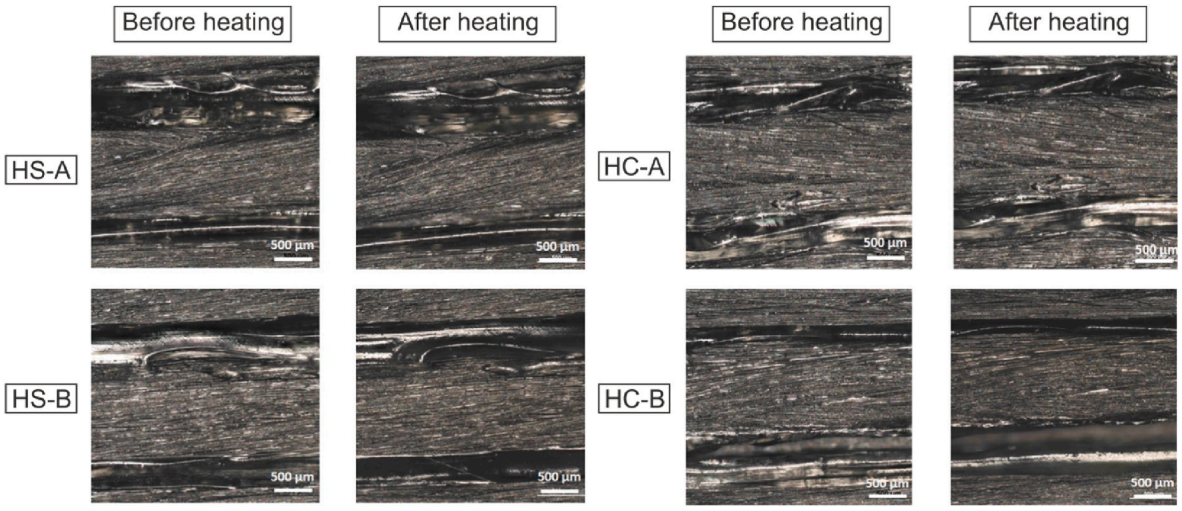

Fig. 11. Optical micrographs of the specimen before and after the prolonged temperature at 65 °C (HS-A) and 145 °C(HS-B); and cyclic temperature between 50 and 70 °C (HC-A) and between 140 and 150 °C (HC–B).

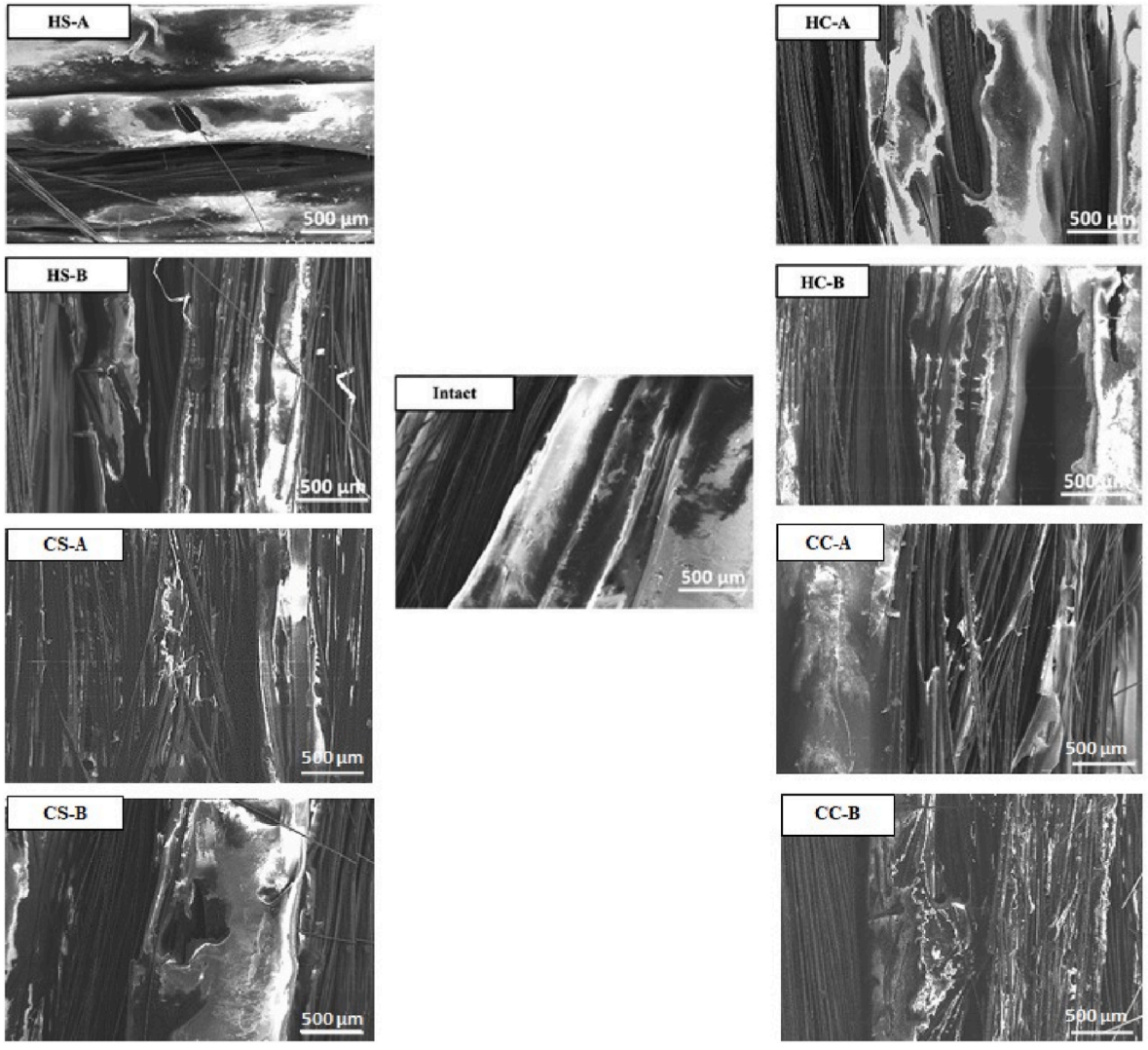

Fig. 12. SEM photos of the untreated and treated specimen group following destructive tensile testing.

underwent significant structural degradation, evidenced by a conspicuous fracture bisecting the material. This fracture observed prominently along the middle, suggests that the polymer experienced considerable stress and strain during the cyclic heating process, resulting in macroscopic damage. Conversely, samples subjected to cyclic thermal treatment between 140 and 150 °C (HC–B) displayed larger and more evenly distributed fractures in the polymer matrix. After prolonged thermal exposure to 145 °C (HS–B), the sample exhibited matrix thinning and larger, more widespread cracks. In contrast, the polymer parts treated with prolonged temperature at 65 °C (HS-A) displayed microcracks, indicating localized weakening within the material. The occurrence of microcracks implies that the PLA underwent thermal expansion or contraction, leading to stress concentrations and subsequent crack formation. These findings underscore the sensitivity of PLA to temperature fluctuations and the importance of controlled processing conditions in ensuring material integrity.

The higher temperatures during cyclic and prolonged thermal treatments (HC–B and HS-B), exacerbate the damage to polymer components. This indicates that elevated temperatures intensify the degradation process, leading to more severe structural damage in the polymer material. The fracture appeared to exist uniformly in almost all areas of the matrix material. In addition to that the fibers were also showing some warping behavior and were no longer coated by the material made from the pre-impregnation process. This can be interpreted as the brittleness observed in the material treated at higher temperatures can be primarily attributed to the increase in crystallinity. Crystallinity restricts the polymer chains' movement, making the material less flexible and more prone to brittle failure. This behavior is confirmed by DSC results where the cold crystallization was not presented in groups HC-A and HC-B. This is because there is no crystal nucleation which will increase the chain mobility with the increasing temperature. In the cold thermal treatment case, the prolonged temperature CS-B created some noticeable gaps in the fibers, and matrix crack was also presented with some fiber pull-out. For the treatment CS-A, fibers seemed to remain in their initial arrangement and the gaps between fibers were not observed. However, the PLA matrix is slightly distorted compared to the untreated (intact) group. Fibers warping and separation were the damage resulting from thermal cycling CC-A. The matrix was observed to be deformed into some unstructured arrangement. A similar morphological structure was observed for the thermal cycling CC-B where the polymer matrix was not only deformed but seemed to be more nucleated and formed some thin-small membranes.

Samples subjected to high-temperature treatments exhibited signs of fiber-matrix debonding and matrix degradation, which are consistent with the observed reductions in mechanical strength and Young's modulus. The morphological features provide a visual confirmation of the damage mechanisms inferred from the DSC and tensile test results. The fracture surfaces of the tensile-tested samples revealed different failure modes depending on the thermal treatment. Samples treated at higher temperatures showed brittle fracture characteristics with less fiber pull-out, indicating reduced ductility and toughness. This morphological evidence supports the findings from both the DSC and tensile analyses, illustrating how thermal history impacts the fracture behavior of CFRP materials. A list of the dominant degradation types for each analysed thermal treatment together with the mechanical parameters values is presented in Table 7.

Table 7
Mechanical parameters, temperature values and the observable degradation types.

Thermal group	Tensile strength [MPa]	Young's Modulus [GPa]	Tg [°C]	Degradation types
Intact	226.14 ± 11.43	28.65 ± 1.14	64.88	Pristine, no polymer damage/fracture
HS-A	217.99 ± 8.44	25.39 ± 1.45	61.58	Localized micro-crack of matrix
HS-B	221.21 ± 6.69	23.97 ± 3.54	63.23	Matrix thinning and more distributed crack of matrix
HC-A	204.41 ± 8.07	20.75 ± 2.55	65.43	Macro-fracture at the middle area of matrix
HC-B	215.49 ± 9.61	25.34 ± 2.31	64.19	Widespread area of matrix fracture
CC-A	216.80 ± 10.05	23.99 ± 1.97	64.73	Fibers warping and separation
CC-B	188.32 ± 8.05	21.60 ± 3.05	64.61	Fibers warping and nucleated matrix
CS-A	209.36 ± 6.97	23.05 ± 1.01	64.33	No fiber pull-out and gaps, matrix brittleness
CS-B	188.93 ± 8.54	22.67 ± 2.39	62.55	Fibers pull-out and gaps, matrix crack

5. Conclusion

This study comprehensively examined the effects of various thermal treatments on the mechanical properties, thermal stability, and morphological characteristics of continuous carbon fiber reinforced polymer (CFRP) composites 3D-printed using the modified FDM printer. Untreated CFRP samples exhibited the highest tensile strength and Young's modulus, indicating superior mechanical performance. Thermal treatments, especially prolonged heating at 145 °C (HS–B) and cyclic thermal exposure between 140 and 150 °C (HC–B), resulted in significant degradation of mechanical properties, as evidenced by reduced tensile strength and modulus. Differential Scanning Calorimetry (DSC) analysis revealed that thermal treatments influenced the glass transition temperature (Tg), crystallinity, and other thermal transitions. Higher Tg values were observed in untreated samples, correlating with better thermal stability and mechanical integrity.

Optical and scanning electron microscopy (SEM) revealed distinct morphological changes in the treated samples. Scanning electron microscopy (SEM) highlighted considerable structural changes in the matrix-fiber interface, such as matrix thinning, cracks, and fiber pull-out. High-temperature treatments (HS–B and HC-B) led to severe and widespread matrix and fiber damage, while cold thermal treatment at −20 °C (CS–B) resulted in noticeable gaps and cracks. SEM analysis indicated that untreated samples maintained an intact and undamaged structure, whereas treated samples, especially those exposed to cyclic heating, showed significant structural degradation, such as macro-fractures and large, widespread cracks.

Thermal treatments significantly impact the crystallinity and thermal stability of the material, which in turn affects its mechanical performance and structural integrity. The increased brittleness and reduced mechanical strength of thermally treated samples are directly linked to the morphological damage observed through SEM and the thermal behavior characterized by DSC. DSC analysis indicated variations in Tg among samples subjected to different thermal treatments. Lower Tg values are associated with decreased polymer chain mobility, suggesting reduced thermal stability. This stability is crucial as it correlates with degraded mechanical properties, where materials with lower Tg demonstrate weaker resistance to deformation under thermal stress. These findings emphasize the need for optimized thermal management in the processing and application of CFRP composites to maintain their mechanical properties and ensure long-term performance. Understanding the effects of thermal treatments provides valuable insights for the design and manufacturing of high-performance composite materials.

CRediT authorship contribution statement

Isyna Izzal Muna: Conceptualization, Methodology, Software, Formal analysis, Investigation, Data curation, Writing – original draft. **Magdalena Mieloszyk:** Conceptualization, Methodology, Validation, Software, Investigation, Resources, Supervision, Funding acquisition, Project administration, Writing – review & editing. **Ruta Rimasauskiene:** Conceptualization, Methodology, Investigation, Resources,

Supervision, Writing – review & editing.

Declaration of competing interest

The authors declare that they have no known competing financial interests or personal relationships that could have appeared to influence the work reported in this paper.

Acknowledgement

The research was financed by the National Science Centre, Poland in the project entitled Thermal Degradation Processes of additively manufactured structures (2019/35/O/ST8/00757), and the Polish National Agency for Academic Exchange in the Foreign Doctoral fellowship (PPN/STA/2021/1/00006).

References

[1] Abdullah F, Okuyama Ki, Morimitsu A, Yamagata N. Effects of thermal cycle and ultraviolet radiation on 3d printed carbon fiber/polyether ether ketone ablator. Aerospace 2020;7:95.
[2] Al Noman A, Kumar BK, Dickens T. Field assisted additive manufacturing for polymers and metals: materials and methods. Virtual Phys Prototyp 2023;18: e2256707.
[3] Bettini P, Alitta G, Sala G, Di Landro L. Fused deposition technique for continuous fiber reinforced thermoplastic. J Mater Eng Perform 2017;26:843–8.
[4] De Leon A, Sweat R. Interfacial engineering of cfrp composites and temperature effects: a review. Mech Compos Mater 2023;59:419–40.
[5] Gracia-Fernández CA, Gómez-Barreiro S, López-Beceiro J, Naya S, Artiaga R. New approach to the double melting peak of poly (l-lactic acid) observed by dsc. J Mater Res 2012;27:1379–82.
[6] Handwerker M, Wellnitz J, Marzbani H, Tetzlaff U. Annealing of chopped and continuous fibre reinforced polyamide 6 produced by fused filament fabrication. Compos B Eng 2021;223:109119.
[7] Harris L. A Study of the crystallisation kinetics in PEEK and PEEK composites. University of Birmingham; 2011. Ph.D. thesis.
[8] Lafarie-Frenot M, Ho N. Influence of free edge intralaminar stresses on damage process in CFRP laminates under thermal cycling conditions. Compos Sci Technol 2006;66:1354–65.
[9] Liu Y, Sing SL. A review of advances in additive manufacturing and the integration of high-performance polymers, alloys, and their composites. Mater Sci Addit Manuf 2023;2:1587.
[10] Maqsood N, Rimašauskas M. Characterization of carbon fiber reinforced pla composites manufactured by fused deposition modeling. Composites Part C: Open Access 2021;4:100112.
[11] Muna II, Mieloszyk M. Temperature influence on additive manufactured carbon fiber reinforced polymer composites. Materials 2021;14:6413.
[12] Muna II, Mieloszyk M, Rimasauskiene R, Maqsood N, Rimasauskas M. Thermal effects on mechanical strength of additive manufactured CFRP composites at stable and cyclic temperature. Polymers 2022;14:4680.
[13] Muravyev NV, Vyazovkin S. The status of pyrolysis kinetics studies by thermal analysis: quality is not as good as it should and can readily be. Thermo 2022;2: 435–52.
[14] Parmar H, Khan T, Tucci F, Umer R, Carlone P. Advanced robotics and additive manufacturing of composites: towards a new era in industry 4.0. Mater Manuf Process 2022;37:483–517.
[15] Pascual-González C, San Martín P, Lizarralde I, Fernández A, León A, Lopes C, Fernández-Blázquez J. Post-processing effects on microstructure, interlaminar and thermal properties of 3d printed continuous carbon fibre composites. Compos B Eng 2021;210:108652.
[16] Paul R, Dai L. Interfacial aspects of carbon composites. Compos Interfac 2018;25: 539–605.
[17] Perez-Martin H, Mackenzie P, Baidak A, Brádaigh CMÓ, Ray D. Crystallinity studies of PEKK and carbon fibre/pekk composites: a review. Compos B Eng 2021; 223:109127.
[18] Rimašauskas M, Kuncius T, Rimašauskiene R. Processing of carbon fiber for 3d printed continuous composite structures. Mater Manuf Process 2019;34:1528–36.
[19] Rubino F, Nisticò A, Tucci F, Carlone P. Marine application of fiber reinforced composites: a review. J Mar Sci Eng 2020;8:26.
[20] Snyder AD, Phillips ZJ, Turicek JS, Diesendruck CE, Nakshatrala KB, Patrick JF. Prolonged in situ self-healing in structural composites via thermo-reversible entanglement. Nat Commun 2022;13:6511.
[21] Su T, Zhou H, Wang R, Chen Y, Luo W, Li M. Effects of working temperature on mechanical performance and failure characteristics of carbon fiber reinforced plastic and adhesive–repaired titanium structures with central inclined cracks. J Mater Eng Perform 2023;32:1824–39.
[22] Swanson TD, Birur GC. Nasa thermal control technologies for robotic spacecraft. Appl Therm Eng 2003;23:1055–65.
[23] Tian X, Liu T, Yang C, Wang Q, Li D. Interface and performance of 3d printed continuous carbon fiber reinforced PLA composites. Compos Appl Sci Manuf 2016; 88:198–205.
[24] Tikhomirova E, Sidokhin Å. Thermal cyclic material tests planning. Strength Mater 2018;50:295–301.
[25] Turnbull D. Formation of crystal nuclei in liquid metals. J Appl Phys 1950;21: 1022–8.
[26] Van Den Einde L, Zhao L, Seible F. Use of frp composites in civil structural applications. Construct Build Mater 2003;17:389–403.
[27] Vorderbrüggen J, Meschut G. Investigations on a material-specific joining technology for cfrp hybrid joints along the automotive process chain. Compos Struct 2019;230:111533.
[28] Zarrelli M, Skordos AA, Partridge IK. Toward a constitutive model for cure-dependent modulus of a high temperature epoxy during the cure. Eur Polym J 2010;46:1705–12.
[29] Zotti A, Zuppolini S, Tábi T, Grasso M, Ren G, Borriello A, Zarrelli M. Effects of 1d and 2d nanofillers in basalt/poly (lactic acid) composites for additive manufacturing. Compos B Eng 2018;153:364–75.